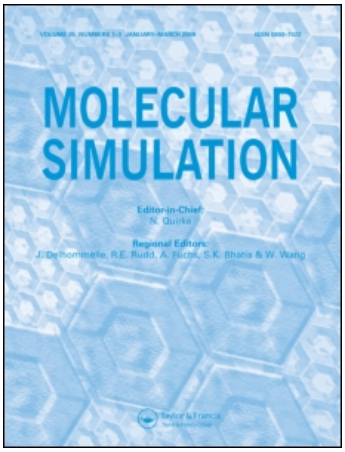

Molecular Simulation
Publication details, including instructions for authors and subscription information:
http://www.informaworld.com/smpp/title~content=t713644482

Modelling of bitumen fragment adsorption on Cu^+ and Ag^+ exchanged zeolite nanoparticles

Stanislav R. Stoyanov[ab]; Sergey Gusarov[a]; Andriy Kovalenko[a]
[a] National Institute for Nanotechnology, National Research Council of Canada, Edmonton, Canada [b] Department of Mechanical Engineering, University of Alberta, Edmonton, Canada

To cite this Article Stoyanov, Stanislav R. , Gusarov, Sergey and Kovalenko, Andriy(2008) 'Modelling of bitumen fragment adsorption on Cu^+ and Ag^+ exchanged zeolite nanoparticles', Molecular Simulation, 34: 10, 943 — 951
To link to this Article: DOI: 10.1080/08927020802101742
URL: http://dx.doi.org/10.1080/08927020802101742

Molecular Simulation
Vol. 34, Nos. 10–15, September–December 2008, 943–951

Taylor & Francis
Taylor & Francis Group

Modelling of bitumen fragment adsorption on Cu^+ and Ag^+ exchanged zeolite nanoparticles

Stanislav R. Stoyanov[ab], Sergey Gusarov[a] and Andriy Kovalenko[ab]*

[a]*National Institute for Nanotechnology, National Research Council of Canada, Edmonton, Canada;* [b]*Department of Mechanical Engineering, University of Alberta, Edmonton, Canada*

(*Received 31 January 2008; final version received 28 March 2008*)

We investigate bitumen desulfurisation on zeolite chabazite nanoparticles that contain Ag^+ and Cu^+ by using periodic density functional theory. The large bitumen molecules that contain thiophene derivative impurities and useful aromatic hydrocarbons cannot enter into zeolite pores but adsorb on the outer surface of the zeolite. The zeolite nanoparticle surface can be optimised for efficient impurities removal and bitumen upgrading, as we have shown recently. On chabazite nanoparticle surface, Ag^+ that reside near the main channel enhance the bitumen fragment adsorption in the order benzene < thiophene < benzothiophene < dibenzothiophene. For Cu^+, the bitumen fragment adsorption strength increases in the order benzene < dibenzothiophene < benzothiophene < thiophene. The different trends arise from the spatial constraint of the surface termination and the smaller ionic radius of Cu^+ relative to Ag^+. Our results show that zeolite surface modifications allow for stronger adsorption of thiophenes relative to hydrocarbons. Our results can be applied toward the rational design of zeolite nanoparticles for bitumen upgrading. We conclude that the preferred configurations of organic macromolecules adsorbed on zeolite outer surfaces can be safely predicted by using Fukui functions.

Keywords: bitumen; desulfurisation; zeolite nanoparticle; ion exchange; periodic DFT

1. Introduction

Canada has extensive bitumen resources that are at a par with Saudi Arabia's conventional oil reserves [1]. Oil sands are unconsolidated deposits of very heavy hydrocarbon bitumen and require multiple stages of processing before refining [2]. Bitumen molecules contain highly unsaturated hydrocarbons and large amounts of chemical impurities, such as sulfur, nitrogen, nickel and vanadium. Bitumen upgrading requires complex catalysts and special reaction conditions. Zeolites are well-known adsorbents and are used for size-selective cracking of hydrocarbons in zeolite pores [3]. The large bitumen molecules cannot enter the zeolite pores but mainly adsorb on zeolite surfaces, which has tremendous potential for bitumen upgrading. Ng et al. have demonstrated that zeolite Y-based catalyst containing active matrix decreases the *N* and *S* contents while increasing the vacuum gas oil conversion rate [4]. Zeolite-based catalytic *nanoparticles* can be derived from inexpensive natural minerals by engineering their surface nanostructure, so as to coordinate, purify and crack the large and complex bitumen molecules [5]. Their reactive surface nanostructure is modified to have large accessible area and to provide highly specific attachment of bitumen fragments. Zeolite-based catalysts derived from inexpensive natural minerals optimised by modifying the zeolite reactive surface can be used for efficient bitumen cracking, removing undesired additives and extraction. Recently, Kuznicki et al. have reported that the catalytic and adsorptive properties of the modified natural zeolite chabazite reduce bitumen viscosity dramatically and remove much of the metals, sulfur and nitrogen at 400°C [5].

A crucial factor in bitumen upgrading is the precise control of reaction conditions. Bitumen hydrotreatment tests performed in *critical conditions* show superior performance with enhanced hydrogen transport to the catalyst surface and reduced zeolite coking, thus promoting the desired reaction pathways [6]. For modelling of processes in *critical conditions*, our group has implemented the 3D reference interaction site model (3D-RISM) theory [7] in the Amsterdam density functional quantum chemistry software package [8,9]. The Kohn–Sham density functional theory (DFT) formalism is coupled to the 3D-RISM integral equation with the Kovalenko–Hirata (KH) closure [10]. This development allows one to model chemical reactions in solution described by *NVT* ensemble (N = number of particles, V = volume, T = temperature). Another promising task is modelling of chemical reaction control by using external electric field. Nanoscale control of ion adsorption and desorption by using homogenous electric fields has been demonstrated by us [11]. This idea can be extended to catalytic control of chemical reactions, including bitumen upgrading on the surface of zeolite nanoparticles.

The preferred sites for metal ions in zeolite frameworks have been investigated by using different theoretical methods. Monte Carlo simulated annealing

*Corresponding author. Email: andriy.kovalenko@nrc-cnrc.gc.ca

ISSN 0892-7022 print/ISSN 1029-0435 online

DOI: 10.1080/08927020802101742
http://www.informaworld.com

modelling results of Na^+ sitting in mordenite are in a very good agreement with experimental results [12]. First-principles molecular dynamics simulation of metal cations in the zeolite offretite has shown that Cu^+ is more tightly bound than alkali metals [13]. Zakharov et al. have modelled the decomposition of NO in a small zeolite cluster that contains Cu^+ [14]. High level cluster Møller-Plesset (MP2) calculations indicate both NO and N_2O bind stronger to Cu^+ exchanged zeolite than to Ag^+ [15]. A number of recent reports make use of DFT codes. Civalleri et al. have applied periodic DFT as implemented in the CRYSTAL code [16] to the investigation of Li^+, Na^+ and K^+ preferred sites in bulk chabazite [17]. These alkali ions form very weak covalent bonds with O atoms. On the other hand, transition metal ions, such as Cu^+, form strong covalent bonds to one or several zeolite framework O atoms [18]. Benco et al. apply the Vienna *ab initio* simulation package (VASP) code [19] and report that Cu^+ and Ag^+ represent particularly strong centres for H_2 adsorption in mordenite channels [20].

Global and local reactivity indices based on DFT provide a highly accurate insight in the reaction site preference prediction that comes at low computational cost [21,22]. Fukui functions have been applied for prediction of inorganic [23,24] and organic reaction sites [25]. In a periodic DFT study using the DMol^3 code, the effect of organic moieties incorporation in chabazite framework on Brønsted acidity has been investigated using several reactivity descriptors [26]. Chatterjee has proposed a semi-quantitative scale for correlation of Brønsted and Lewis acidity for a range of bi- and trivalent-metal dopants in aluminophosphates [27]. Bifunctional acid–base catalysed reactions in zeolites have been modelled using the principle of maximum hardness [28]

The theoretical reports on thiophene adsorption on zeolites are limited to cluster models. DFT studies suggest that the thiophene cracking reaction could be catalysed by Lewis instead of Brønsted sites [29]. The weak interaction between thiophene and zeolite cluster Brønsted sites has been shown to lead to the formation of van der Walls complexes [30]. Yang et al. have shown by elution experiment and DFT calculation of a small zeolite cluster that Cu^+ and Ag^+ exchanged zeolite Y selectively adsorbs both sulfur- and nitrogen-containing heterocycles from diesel fuels under ambient conditions [31,32]. Nitrogen-containing heterocycles reduce the fuel desulfurisation capacity of Cu(I)Y zeolite because of competitive adsorption [33,34].

We have recently presented a periodic DFT (DMol^3) and quantum mechanics/molecular mechanics investigation of zeolite nanoparticle acidity, in particular zeolite surface acidity. Our periodic DFT results suggest that aluminum substitution near chabazite 'open' surface creates stable acid sites that are accessible to bitumen fragments. The most stable Brønsted sites contain protons at the O1 and O3 positions for both bulk and slab chabazite models, in agreement with the experiment. Fukui functions are applied for nanoparticle reactivity prediction and are considered useful for the development of surface reactivity maps that could be applied for the design of nanoparticles with optimal functionality [35]. Here, we model the adsorption of sulfur-containing bitumen fragments on these metal ion-exchanged nanostructures. We also investigate the preferred sites for ion-exchange of Ag^+ and Cu^+ on zeolite chabazite nanoparticles.

2. Computational technique

For the periodic DFT modelling using the DMol^3 software from Accelrys Materials Studio® 4.0, San Diego, CA, USA, [36], we employ the PW91 density functional [37]. Geometries optimised using the PW91 (Perdew–Wang, 1991) functional are in a better agreement with the experiment than these from other functionals, such as the widely-used B3LYP functional [38,39]. It has also been shown that PW91 is capable of modelling van der Waals interactions, although dispersive interactions are not physically included in it [40]. We use the all-electron double numerical basis set with polarisation function (DNP [41]). The DNP basis set is comparable to the 6-31G2mu** basis set. However, the numerical basis set performs better than a Gaussian basis set of the same size for molecules, semi-conductors and insulators [42]. Brillouin-zone sampling is restricted to the Γ point because the zeolite slab is an insulator and sampling of the five slab irreducible *k*-points changes the E_{ADS} values by less than 1 kJ/mol. Also, Fukui function calculations are not enabled for multiple *k*-points in DMol^3. We have employed the extra-fine numerical integration grid that contains 474 angular points. The number of radial points is a function of the nuclear charge and varies with the periodic system size [41,43]. The electronic singlet states are treated using single determinants. The initial periodic unit cell zeolite geometries are obtained from the Accelrys Materials Studio [36] database and fully optimised. The chabazite lattice parameters are taken from the X-ray report [44] and are not optimised. The real space cutoff for the atomic numerical basis set calculation has been set to 4.0 Å. The geometry optimisation convergence is achieved when the energy, gradient and displacement are lower than 1×10^{-5} Ha, 1×10^{-3} Ha/Å and 1×10^{-3} Å, respectively.

3. Ion exchange

The metal ion exchange of zeolite Brønsted protons leads to the formation of Lewis acid sites that are the strongest adsorption centres in zeolites. Lewis sites exhibit the highest adsorption energies [45] and molecules adsorbed on these sites yield the largest molecular stretching mode

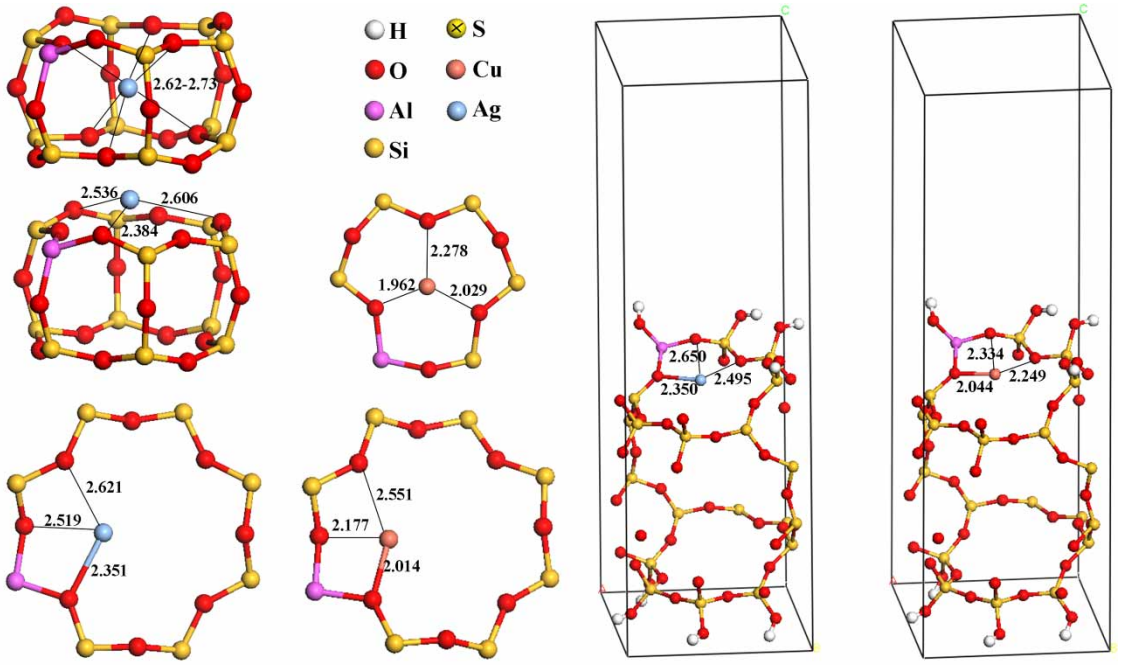

Figure 1. The Ag^+ and Cu^+ exchanged bulk (left) and slab chabazite (right).

frequency shifts [46]. This is because the coordination by zeolite framework O atoms cannot provide complete coordination to the metal ions. Thus, cations move closer to the framework and exhibit extraordinary adsorption power [16]. Metal cations can be reduced and form metal clusters embedded in the zeolite framework [47,48]. The interaction between metal cations and zeolites is a combination of three factors: covalent bonding between the cation and the framework O atoms, electrostatic bonding between the cation and the partially ionic O atoms adjacent to the Al substitution site and electrostatic interaction between the cation and the positively charged Al centre [17].

In Figure 1 (left), we show the preferred sites for Ag^+ and Cu^+ in bulk chabazite. For Ag^+, we found three preferred sites – near the centre of the six-membered ring, near the centre of the hexagonal prism and in the eight-membered ring, with relative energies of 0, −2 and −4 kJ/mol, respectively. These small energy differences show that the three sites have similar stability. For comparison, X-ray crystallographic determination of fully Ag^+ exchanged chabazite with Si/Al ratio of 2.18 also found Ag^+ in these three sites [49]. The bond alternation determined from the X-ray [49] is in agreement with our modelling results. For Cu^+, we found two preferred sites – near the centre of the six-membered ring and in the eight-membered ring, with relative energies of −43 and 0 kJ/mol, respectively. Analysis of Cu K-edge X-ray adsorption spectroscopy data for Cu^+ exchanged faujasite has given average Cu—O distance of 1.99 Å [50]. This value is in a relatively good agreement with our modelling results. For comparison, Solans-Monfort et al. report two Cu^+ preferred sites from periodic DFT calculations. These authors obtain Cu—O bond lengths of 2.02, 2.10 and

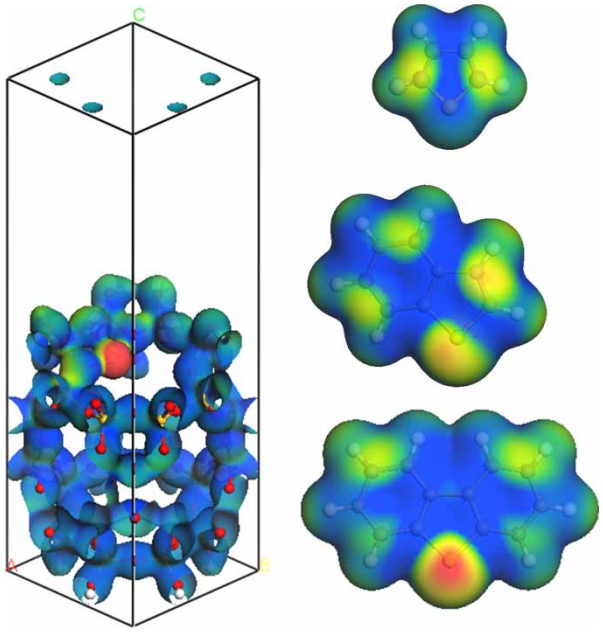

Figure 2. Nucleophilic Fukui function of Cu^+ exchanged chabazite slab (left), electrophilic Fukui functions of thiophene, benzothiophene and dibenzothiophene (right) mapped on the $0.02e/Å^3$ electron density surface.

2.25 Å near the centre of the six-membered ring, whereas, in the eight-membered ring the Cu—O bond lengths are 2.06 and 2.22 Å. These authors also found that Cu^+ in the eight-membered ring acts as a stronger H_2 adsorbent than near the centre of the six-membered ring [18]. The B3LYP functional employed in the latter study is known to yield longer metal-ligand bonds relative to the experiment [51].

We have modelled Brønsted acid sites on chabazite nanoparticle surface by using periodic cells designed by termination along the (00-3) and (003) planes and Al substitution. Our results have shown that the most stable structure contains Al on the surface and has a periodic cell designed from $1 \times 1 \times 1.6$ chabazite unit cells ($9.42 \times 9.42 \times 15$ Å) cut along the (003) plane and a 13.3 Å thick vacuum slab [35]. We also found that the most stable Brønsted site contains a proton in the eight-membered ring near the surface termination [35]. This is important because we expect that bitumen fragment adsorption would occur on the chabazite surface due to the large fragment size. Hence, we selected this site for the bitumen fragment adsorption modelling.

In Figure 1 (right), we show the optimised geometry of Ag^+ and Cu^+ exchanged at the most stable Brønsted site. Metal ions exchanged on this site are undercoordinated and would be highly adsorptive [16]. It is interesting to note that within the eight-membered surface pore mouth Cu^+ forms three Cu—O bonds compared to two for the bulk. Calligaris et al. describe several coordination configurations of Ag^+ in the eigth-membered ring that resemble our slab model [49]. Overall, the slab Cu—O and Ag—O bond lengths are slightly longer than in bulk because of the reduced structure rigidity near the surface termination.

4. Prediction of bitumen fragment adsorption configuration

We predict bitumen fragment adsorption configurations by using global softness and Fukui functions. Using the finite difference approximation, the global softness is evaluated as $S = 1/(\mathrm{IP} - \mathrm{EA})$, where IP is the ionisation potential and EA is the electron affinity [52,53]. In this work, for a neutral system that contains N electrons, we obtain:

$$S = \frac{0.1}{(E_{(N-0.1)} - E_{(N)}) - (E_{(N)} - E_{(N+0.1)})}, \qquad (1)$$

where $E_{(N-0.1)}$, $E_{(N)}$ and $E_{(N+0.1)}$ are the ground state energies of the system with $N - 0.1$, N and $N + 0.1$ electrons, respectively.

The Fukui function is motivated by the following consideration: if a fraction of an electron δ is transferred to an N electron molecule, it will tend to distribute so as to minimise the energy of the resulting $N + \delta$ electron system [54]. The resulting change in electron density $(\delta\rho(r)/\delta N)^+_{v(r)}$ defined in Equation (2) is the nuleophilic Fukui function. In analogy, the $(\delta\rho(r)/\delta N)^-_{v(r)}$ defined in Equation (3) is the electrophilic Fukui function. In this work, we use δ values of 0.1 and -0.1 electrons. It is notable that there are similarities between the interpretation of the Fukui functions and the frontier molecular orbital theory proposed by Fukui [55,56].

$$f^+_N(r) = (\delta\rho(r)/\delta N)^+_{v(r)} = \rho_{(N+0.1)}(r) - \rho_{(N)}(r), \qquad (2)$$

$$f^-_N(r) = (\delta\rho(r)/\delta N)^-_{v(r)} = \rho_{(N)}(r) - \rho_{(N-0.1)}(r), \qquad (3)$$

where $\rho_{(N-0.1)}(r)$, $\rho_N(r)$ and $\rho_{(N+0.1)}(r)$ are the electron densities of the system with $N - 0.1$, N and $N + 0.1$ electrons, respectively, all evaluated at the optimised geometry of the N electron system.

In the finite difference approximation, the condensed Fukui functions [53] of atom x in a molecule that contains N electrons are defined in Equations (4) and (5).

$$f^+_x = 10[q_x(N + 0.1) - q_x(N)] \quad \text{(for nucleophilic attack)}, \qquad (4)$$

$$f^-_x = 10[q_x(N) - q_x(N - 0.1)] \quad \text{(for electrophilic attack)}, \qquad (5)$$

where q_x is the charge of atom x. For q_x calculation, we employ the Hirshfeld [57] and Mulliken population analysis [58] methods. A more detailed discussion on reactivity indices is presented elsewhere [35].

In Figure 2, we show the Fukui functions for slab and bitumen fragments mapped on the electron density isosurface. The Fukui function maxima and minima are mapped in red and blue, respectively. The nucleophilic Fukui function map of our Cu^+ exchanged chabazite model slab suggests the reaction configuration preference towards an attack by a nucleophile, such as a bitumen fragment. The red region at the Cu atom indicates that this is the preferred nucleophilic attack site. The yellow-green region at the hydroxyl nest (shown towards the back) indicates that this is a less preferred site, whereas the remainder of the slab that is colored in blue is not a preferred site. Next, we consider the bitumen fragment reactivity preferences suggested by the electrophilic Fukui function maps. For thiophene, the preferred sites are the C atoms adjacent to the S atom. For benzo- and dibenzothiophene, the most preferred sites are the S atoms and less preferred sites are the C atoms located at the yellow-colored map regions. Thus, the preferred dibenzothiophene configuration would be at a small angle relative to the slab xy plane. This way, the S atom would interact with the metal atom and the C atoms would interact with the hydroxyl nest for maximum overlap. The Fukui functions provide suggestions for the preferred adsorption configuration at the low computational cost

of a single point calculation at the optimised geometry of the reactants. For comparison, configuration sampling could be obtained from quantum molecular dynamics at much higher computational cost.

In Table 1, we list selected reactivity indicators for Cu^+ and Ag^+ exchanged slabs as well as bitumen fragments. The global softness (S) values show of the Cu^+ exchanged slab is higher than that of the Ag^+ slab, indicating that Cu^+ would be more reactive towards soft nucleophiles. The bitumen fragment global softness increases in the order benzene $<$ thiophene $<$ benzothiophene $<$ dibenzothiophene. We expect that the strength of bitumen fragment adsorption would also increase in this order.

Condensed Fukui functions provide quantitative predictions on reaction regioselectivity. In the metal cation exchanged slabs, both f^- and f^+ of Cu^+ are higher than for the other atoms. Also, the values of f^- and f^+ are comparable, with the Hirshfeld method yielding higher f^- and Mulliken – higher f^+. This clearly suggests that Cu^+ can act as both electron donor and electron acceptor, as it is well know from the disproportionation reaction $2Cu^+ \rightarrow Cu^0Cu^{2+}$. For Ag^+ in slab, we obtain f^+ value that is much higher than f^-, indicating that Ag^+ is a hard acid.

The bitumen fragment condensed Fukui functions could help us to predict their reactivity. For thiophene, the S atom f^+ and f^- values are higher than the C atom adjacent to S (C1). These values suggest that thiophene could react with S or C1 atom, depending on reactivity of the other reactant. The partitioning of the molecular Fukui function to condensed (atomic) Fukui functions is strongly dependent on the population analysis method used. The performance of different condensed Fukui function calculation methods are discussed elsewhere [35,59]. For benzo- and dibenzothiophene, the S atom f^- values are larger than the respective f^+ values. The highest bitumen fragment f^- values increase in the order benzene $<$ thiophene $<$ benzothiophene $<$ dibenzothiophene, giving a predicted reactivity order. The reaction sites locations predicted from these values are in good agreement with the optimised structures of adsorbed thiophenes, as discussed below.

Table 1. Global softness (S) and condensed nucleophilic (f^+) and electrophilic (f^-) Fukui functions for metal ion exchanged chabazite slab and bitumen fragments. The condensed Fukui function values are calculated by using Hirshfeld (Mulliken) population analysis.

	S, (Ha^{-1})	f^+	f^-
Cu (Cu-slab)	8.94	0.515 (0.648)	0.562 (0.567)
Ag (Ag-slab)	7.22	0.612 (0.722)	0.076 (0.077)
Cu (CuCl)	9.99	0.722 (0.729)	0.570 (0.573)
Ag (AgCl)	9.25	0.739 (0.753)	0.418 (0.428)
S (thiophene)	5.49	0.257 (0.253)	0.187 (0.197)
C1 (thiophene)	–	0.139 (0.116)	0.170 (0.122)
S (benzothiophene)	6.73	0.146 (0.162)	0.223 (0.238)
S (dibenzothiophene)	7.50	0.088 (0.114)	0.242 (0.259)
C (benzene)	4.90	0.106 (0.064)	0.110 (0.061)

5. Bitumen fragment adsorption

In bitumen, sulfur is present primarily as thioethers, sulfides and thiophene derivatives, with thiophene sulfur being particularly difficult to remove by hydrodesulfurisation [31]. Transition metal ion-exchanged natural zeolites could be used as economical and disposable materials for bitumen desulfurisation [5].

In Figure 3, we show the optimised geometries and selected optimised bond length of bitumen fragments on Cu^+ and Ag^+ exchanged chabazite slabs that we show in Figure 1 (right). The bitumen fragment adsorption to the two metal atoms occurs in similar configurations. Upon bitumen fragment adsorption, the Cu—O and Ag—O bond lengths become shorter relative to the ion-exchanged slabs shown in Figure 1 (right). The ion-exchanged zeolite adsorption strength is evaluated from the adsorption energy $E_{ADS} = E_{Z-Ion-BF} - E_{Z-Ion} - E_{BF}$. The $E_{Z-Ion-M}$ is the total energy of the ion-exchanged zeolite unit cell with a bitumen fragment adsorbed on it. The E_{Z-Ion} and E_{BF} are the total energies of the ion-exchanged zeolite unit cell and the bitumen fragment, respectively.

The benzene adsorption is relatively weak and does not cause changes in the strong Cu—O and Ag—O bonds (shown as colored sticks), whereas the weak ones (shown as black lines) become slightly shortened. The thiophene bitumen fragment adsorption is stronger than benzene, as demonstrated by the lower E_{ADS} values. For thiophene adsorption, the strong Cu—O and Ag—O bonds become shortened, whereas the weak bonds become elongated. We obtain E_{ADS} values of -150 and -159 kJ/mol for benzene and thiophene on Cu^+ ion-exchanged chabazite, respectively. This result indicates that thiophene adsorption is stronger than benzene. This result is in qualitative agreement with previous small cluster DFT modelling reports [32,33]. The thiophene adsorption configurations to Ag^+ and Cu^+ via the S atom represent local minima on the potential energy surfaces. The optimised geometries of thiophene adsorbed on Cu^+ and Ag^+ exchanged slab via the S atom are 19 and 4 kJ/mol less stable than the respective structures shown in Figure 3. The thiophene adsorption via the C atom adjacent to S is in agreement with the thiophene electrophilic Fukui function prediction.

The benzo- and dibenzothiophene adsorption occurs via the S atoms. Both the metal—O and metal—S bonds are longer for dibenzothiophene relative to benzothiophene. The adsorption energy values for the bitumen fragments in this study suggest stronger adsorption to Cu^+ relative to Ag^+ slabs. This is in agreement with experimental adsorption studies [32]. For the Cu^+ exchanged slab, the

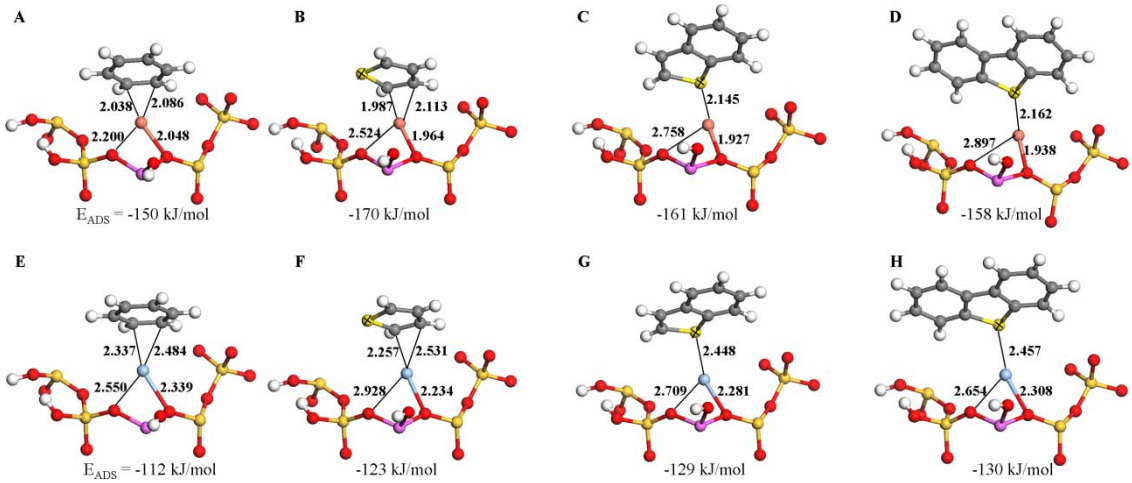

Figure 3. Optimised geometries of benzene and thiophenes adsorbed on the Cu^+ (A–D) and Ag^+ exchanged chabazite slabs (E–H) shown in Figure 1 (right).

E_{ADS} values increase in the order thiophene < benzothiophene < dibenzothiophene < benzene. For the Ag^+ exchanged slab, the E_{ADS} values increase in the order dibenzothiophene < benzothiophene < thiophene < benzene. Our benzene and thiophene adsorption strength orders are in agreement with the experimental results of Yang et al. [34]. The different trends are due to the spatial constraints of the nanoparticle surface binding site. The larger ionic radius of Ag^+ allows it to sit above the pore mouth and provides for more effective adsorption of larger bitumen fragments.

It would be instructive to compare our geometry optimisation results to the report of Yang et al. for thiophene adsorption to CuCl and the zeolite cluster $(OH)_3Si—OCu—Al(OH)_3$ [34]. These authors obtain a cluster Cu—O distance of 2.14 Å that is longer than our value of 2.044 Å (Figure 1 (right)). The thiophene adsorption is modelled via the S atom and the Cu—S distance of 2.50 Å is longer than our value of 2.151 Å. The Cu—S bond lengths for adsorption of benzo- and dibenzothiophene of 2.49 Å are also longer than ours. This could be due to the zeolite framework electron conjugation and long-range electrostatic effects that our periodic model accounts for. It is important to note that the cluster results are strongly dependent on the selection of cluster size and shape [60]. Also, small clusters are not reliable zeolite crystal models especially when the "dangling bonds" are close to adsorbates or any reacting molecule [61]. On the other hand, periodic DFT does not require structure-related selections.

The preferred thiophene adsorption configuration on nanoparticles is not well understood. Sargent and Titus report that the thiophene highest occupied molecular orbital (HOMO) predicted from B3LYP calculations contains the π-component of the C═C bond but not the S atom lone pair, suggesting π-coordination to one or both of the C═C bonds [62]. The lowest unoccupied molecular orbital (LUMO) is π-antibonding with respect to all adjacent atoms except for the distal C—C bond. The metal—S bond formation has been explained by considering a linear combination between the HOMO-1 and HOMO-2 [62]. This frontier orbital description is in agreement with our results. The literature on thiophene adsorption on zeolite surfaces is limited to small zeolite clusters. The long Cu—S distances produced by the cluster approach [34] suggest that more accurate method is needed. Although the thiophene adsorption on Mo sulfide clusters is more extensively studied, the thiophene adsorption mode remains controversial. Frequency response experiments suggest that thiophene is first π-adsorbed on the transition metal ion in the zeolite Y cage and then large amounts of thiophene are adsorbed by directly forming metal—S bonds [63]. Raman and infrared spectroscopic studies suggest that thiophene is adsorbed via the S atom [64].

In Figure 4, we show the HOMOs of Cu^+ exchanged chabazite that contain adsorbed thiophene and benzene. The Cu^+ exchanged chabazite HOMO (left) has Cu d_{xy} and

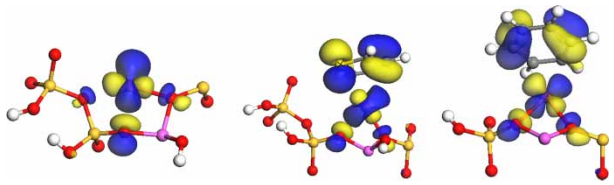

Figure 4. Schematic diagrams of the HOMOs of Cu^+ exchanged chabazite slab (left) that contains adsorbed thiophene (middle) and benzene (right). The entire slab is in Figure 1 (right). Isosurfaces of 0.03 and −0.03 $|e|/Å^3$ are shown in blue and yellow, respectively.

O *p* character. The three Cu—O bonds have σ-antibonding character, as evidenced by the opposite eigenvalue signs, and the O atom with the largest node forms the longest Cu—O bond. Upon adsorption of thiophene (middle), one of the Cu—O bonds breaks. From the Hirshfeld and Mulliken population analysis methods, we obtain that upon adsorption thiophene donates 0.091 and 0.356*e*, respectively. The electron donation from thiophene [62] changes the Cu frontier orbital occupancy. The Cu d_z^2 orbital forms two σ bonds to O atoms and a σ bond to the thiophene C atom adjacent to the S atom. The HOMO of the benzene adsorption (right) has Cu d_{xy} character similar to that of the Cu^+ exchanged chabazite (left) because benzene is a weaker electron donor. From the Hirshfeld and Mulliken population analysis methods, we obtain that upon adsorption benzene donates 0.020 and 0.302*e*, respectively. The Cu d_{xy} orbital forms two σ bonds to O atoms and a π bond to a benzene C═C bond. The thiophene adsorption is stronger because it involves electron donation from thiophene to metal ion, as shown by Sargent and Titus for metal—S coordination [62]. The HOMOs for Ag^+ exchange and adsorption are qualitatively similar.

6. Conclusion

We apply periodic DFT for modelling of the preferred Cu^+ and Ag^+ sites in the bulk and slab of chabazite and the enhanced adsorption of thiophenic bitumen fragments on the slab. We found the following: (1) the preferred sites of Cu^+ exchanged in bulk chabazite are near the centre of the six-membered ring and in the eight-membered ring. In addition to these two sites, Ag^+ occupies the centre of the hexagonal prism; (2) both Cu^+ and Ag^+ are stable at the eight-membered ring pore mouth of the chabazite slab; (3) thiophene adsorbs preferentially to benzene on chabazite slabs that are exchanged with Cu^+ and Ag^+ cations; and (4) the adsorption energies of bitumen fragments on the Ag^+ exchanged chabazite slabs increase in the order benzene < thiophene < benzothiophene < dibenzothiophene. The adsorption energies of bitumen fragments on the Cu^+ exchanged chabazite slabs increase in the order benzene < dibenzothiophene < benzothiophene < thiophene. The overall conclusion is that Fukui functions can be safely used as a guide to find the preferred adsorption configuration of bitumen fragments on transition metal cation exchanged chabazite surfaces. However, local steric effects can alter predicted binding and reactivity trends. We intend to develop a systematic method for description of zeolite nanoparticle surface reactivity toward specific bitumen fragments. Our results can be employed to map zeolite nanoparticles surfaces for selective adsorption of organic macromolecules, including bitumen.

Acknowledgements

This work was supported by Imperial Oil Resources, Centre for Oil Sands Innovation (COSI) at the University of Alberta, and the National Institute for Nanotechnology, National Research Council of Canada. The computations were supported by the Centre of Excellence in Integrated Nanotools at the University of Alberta.

References

[1] E.P. Newell, *Canada's oilsands industry comes of age*, Oil Gas J. 97 (1999), pp. 44–53.
[2] T. Jiang, G. Hirasaki, C. Miller, K. Moran, and M. Fleury, *Diluted bitumen water-in-oil emulsion stability and characterization by nuclear magnetic resonance (NMR) measurements*, Energy Fuels 21 (2007), pp. 1325–1336.
[3] M. Occelli (ed.), *Fluid Catalytic Cracking II: Concepts in Catalyst Design.* ACS Symposium Series, ACS, Washington, DC, 1991.
[4] S. Ng, Y. Zhu, A. Humphries, L. Zheng, F. Ding, L. Yang, and S. Yui, *FCC study of Canadian oil-sands derived vacuum gas oils. 1. Feed and catalyst effects on yield structure and 2. Effects of feedstocks and catalysts on distributions of sulfur and nitrogen in liquid products*, Energy Fuels 16 (2002), pp. 1196–1221.
[5] S.M. Kuznicki, W.C. McCaffrey, J. Bian, E. Wangen, A. Koenig, and C.H. Lin, *Natural zeolite bitumen cracking and upgrading*, Microporous Mesoporous Mater. 105 (2007), pp. 268–272.
[6] D.S. Scott, D. Radlein, J. Piskorz, P. Majerski, and T.J.W. deBruijn, *Upgrading of bitumen in supercritical fluids*, Fuel 80 (2001), pp. 1087–1099.
[7] A. Kovalenko, *Three-dimensional RISM theory for molecular liquids and solid–liquid interfaces*, in *Understanding Chemical Reactivity: Molecular Theory of Solvation*, F. Hirata ed.,Vol. 24, Kluwer Academic Publishers, The Netherlands, 2003, pp. 169–275.
[8] S. Gusarov, T. Ziegler, and A. Kovalenko, *Self-consistent combination of the three-dimensional RISM theory of molecular solvation with analytical gradients and the amsterdam density functional package*, Phys. Chem. A 110 (2006), pp. 6083–6090.
[9] D. Casanova, S. Gusarov, A. Kovalenko, and T. Ziegler, *Evaluation of the SCF combination of KS-DFT and 3D-RISM-KH; solvation effect on conformational equilibria, tautomerization energies, and activation barriers*, J. Chem. Theory Comput. 3 (2007), pp. 458–476.
[10] A. Kovalenko and F. Hirata, *Self-consistent description of a metal–water interface by the Kohn–Sham density functional theory and the three-dimensional reference interaction site model*, J. Chem. Phys. 110 (1999), p. 10095.
[11] S.R. Stoyanov, P. Král, and B. Wang, *Extended electronic states above metal-doped carbon nanostructures*, Appl. Phys. Lett. 90 (2007), pp. 153111–153113.
[12] G. Maurin, P. Senet, S. Devautour, P. Gaveau, F. Henn, V.E. Van Doren, and J.C. Giuntini, *Combining the Monte Carlo technique with 29Si NMR spectroscopy: Simulations of cation locations in zeolites with various Si/Al ratios*, J. Phys. Chem. B 105 (2001), pp. 9157–9161.
[13] L. Campana, A. Selloni, J. Weber, and A. Goursot, *Cation siting and dynamical properties of zeolite offretite from first-principles molecular dynamics*, J. Phys. Chem. B 101 (1997), pp. 9932–9939.
[14] I.I. Zakharov, Z.R. Ismagilov, S. Ph. Ruzankin, V. F. Anufrienko, S.A. Yashnik, and O.I Zakharova, *Density functional theory molecular cluster study of copper interaction with nitric oxide dimer in Cu-ZSM-5 catalysts*, J. Phys. Chem. C 111 (2007), pp. 3080–3089.
[15] N.U. Zhanpeizov, W.S. Ju, M. Matsuoka, and M. Anpo, *Quantum chemical calculations on the structure and adsorption properties of NO and N_2O on Ag^+ and Cu^+ ion-exchanged zeolites*, Struct. Chem. 14 (2003), pp. 247–255.
[16] V.R. Saunders, R. Dovesi, C. Roetti, M. Causà, N.M. Harrison, R. Orlando, and C.M. Zicovich-Wilson, *CRYSTAL-98 User's Manual*, Università di Torino, Italy, 1999.

[17] B. Civalleri, A.M. Ferrari, M. Llunell, R. Orlando, M. Merawa, and P. Ugliengo, *Cation selectivity in alkali-exchanged chabazite: An* ab initio *periodic study*, Chem. Mater. 15 (2003), pp. 3996–4004.

[18] X. Solans-Monfort, V. Branchadell, M. Sodupe, C.M. Zicovich-Wilson, E. Gribov, G. Spoto, C. Busco, and P. Ugliengo, *Can Cu^+-exchanged zeolites store molecular hydrogen? An* ab initio *periodic study compared with low-temperature FTIR*, J. Phys. Chem. B 108 (2004), pp. 8278–8286.

[19] G. Kresse and J. Furthmueller, *Efficient iterative schemes for* ab initio *total-energy calculations using a plane-wave basis set*, Phys. Rev. B 54 (1996), pp. 11169–11186; G. Kresse and J. Hafner, *Ab initio molecular dynamics for open-shell transition metals*, Phys. Rev. B 48 (1993), pp. 13115–13118; G. Kresse and J. Hafner, *Ab initio molecular-dynamics simulation of the liquid–metal–amorphous–semiconductor transition in germanium*, Phys. Rev. B 49 (1994), pp. 14251–14269; G. Kresse and J. Furthmuller, *Efficiency of ab initio total energy calculations for metals and semiconductors using a plane-wave basis set*. Comput. Mater. Sci. 6 (1996), pp. 15–50.

[20] L. Benco, T. Buĉko, J. Hafner, and H. Toulhoat, *A density functional theory study of molecular and dissociative adsorption of H2 on active sites in mordenite*, J. Phys. Chem. B 109 (2005), pp. 22491–22501.

[21] R.K. Roy, S. Krishnamurti, P. Geerlings, and S. Pal, *Local softness and hardness based reactivity descriptors for predicting intra- and intermolecular reactivity sequences: Carbonyl compounds*, J. Phys. Chem. A 102 (1998), pp. 3746–3755.

[22] R.C. Deka, R.K. Roy, and K. Hirao, *Local reactivity descriptors to predict the strength of Lewis acid sites in alkali cation-exchanged zeolites*, Chem. Phys. Lett. 389 (2004), pp. 186–190.

[23] C. Makedonas and C.A. Mitsopoulou, *Introduction of modified electronic parameters – searching for a unified ligand properties scale through the electrophilicity index concept*, Eur. J. Inorg. Chem. 26 (2007), pp. 4176–4189.

[24] L.J. Bartolotti and P.W. Ayers, *An example where orbital relaxation is an important contribution to the Fukui function*, J. Phys. Chem. A 109 (2005), pp. 1146–1151.

[25] D. Guerra, P. Fuentealba, A. Aizman, and R. Contreras, *β-Scission of thioimidoyl radicals (*R*1*-N-*C.bul.* = *S*-*R*2*): A theoretical scale of radical leaving group ability*, Chem. Phys. Lett. 443 (2007), pp. 383–388.

[26] M. Elanany, B.-L. Su, and D.P. Vercauteren, *Strong templating effect of TEAOH in the hydrothermal genesis of the AlPO4-5 molecular sieve: Experimental and computational investigations*, J. Mol. Catal. 270 (2007), pp. 295–301.

[27] A. Chatterjee, *A reactivity index study to rationalize the effect of dopants on Brønsted and Lewis acidity occurring in MeAlPOs*, J. Mol. Graphics Modell. 24 (2006), pp. 262–270.

[28] K. Hemelsoet, D. Lesthaeghe, V. Van Speybroeck, and M. Waroquier, *Bifunctional acid–base catalyzed reactions in zeolites from the HSAB viewpoint*, Chem. Phys. Lett. 419 (2006), pp. 10–15.

[29] X. Rozanska, R.A. van Santen, and F. Hutschka, *A DFT study of the cracking reaction of thiophene activated on zeolite catalysts: The role of the basic Lewis site*, Stud. Surf. Sci. Catal. 135 (2001), pp. 2611–2617.

[30] H. Soscun, O. Castellano, J. Hernandez, and A. Hinchliffe, *Theoretical study of the structural, vibrational, and topologic, properties of the charge distribution of the molecular complexes between thiophene and Brønsted acid sites in zeolites*, Int. J. Quantum Chem. 87 (2002), pp. 240–253.

[31] R.T. Yang, A.J. Hernandez-Maldonado, and F.H. Yang, *Desulfurization of transportation fuels with zeolites under ambient conditions*, Science 301 (2003), pp. 79–81.

[32] A.J. Hernandez-Maldonado, and R.T. Yang, *Desulfurization of liquid fuels by adsorption via π-complexation with Cu(I)-Y and Ag-Y zeolites*, Ind. Eng. Chem. Res. 42 (2003), pp. 123–129.

[33] J. Ambalavanan, F.H. Yang, and R.T. Yang, *Effects of nitrogen compounds and polyaromatic hydrocarbons on desulfurization of liquid fuels by adsorption via π-complexation with Cu(I)Y zeolite*, Energy Fuels 20 (2006), pp. 909–914.

[34] F.H. Yang, A.J. Hernandez-Maldonado, and R.T. Yang, *Selective adsorption of organosulfur compounds from transportation fuels by π-complexation*, Sep. Sci. Technol. 39 (2004), pp. 1717–1732.

[35] S. R. Stoyanov, S. Gusarov, S. M. Kuznicki, and A. Kovalenko, *Theoretical modeling of zeolite nanoparticle surface acidity for heavy oil upgrading*, J. Phys. Chem. C 112 (2008), pp. 6794–6810.

[36] *$DMol^3$, release 4.0*, Accelrys, Inc., CA (2001).

[37] J.P. Perdew, J.A. Chevary, S.H. Vosko, K.A. Jackson, M.R. Pederson, D.J. Singh, and C. Fiolhais, *Atoms, molecules, solids, and surfaces: Applications of the generalized gradient approximation for exchange and correlation*, Phys. Rev. B 46 (1992), pp. 6671–6687.

[38] C. Lo, and B.L. Trout, *Density-functional theory characterization of acid sites in chabazite*, J. Catal. 227 (2004), pp. 77–89.

[39] F. Pascale, P. Ugliengo, B. Civalleri, R. Orlando, P. D'Arco, and R. Dovesi, *Hydrogarnet defect in chabazite and sodalite zeolites: A periodic Hartree–Fock and B3-LYP study*, J. Chem. Phys. 117 (2002), pp. 5337–5346.

[40] S. Tsuzuki, and H.P. Luthi, *Interaction energies of van der Waals and hydrogen bonded systems calculated using density functional theory: Assessing the PW91 model*, J. Chem. Phys. 114 (2001), pp. 3949–3957.

[41] B. Delley, *An all-electron numerical method for solving the local density functional for polyatomic molecules*, J. Chem. Phys. 92 (1990), pp. 508–517.

[42] B. Delley, *From molecules to solids with the $DMol^3$ approach*, J. Chem. Phys. 113 (2000), pp. 7756–7764.

[43] S. Tosoni, F. Pascale, P. Ugliengo, R. Orlando, V.R. Saunders, and R. Dovesi, *Quantum mechanical calculation of the OH vibrational frequency in crystalline solids*, Mol. Phys. 103 (2005), pp. 2549–2558.

[44] M. Calligaris, G. Nardin, L. Randaccio, and P.C. Chiaramonti, *Cation-site location in a natural chabazite*, Acta Crystallogr. B 38 (1982), pp. 602–605.

[45] L. Benco, T. Buĉko, J. Hafner, and H. Toulhoat, Ab initio *simulation of Lewis sites in mordenite and comparative study of the strength of active sites via CO adsorption*, J. Phys. Chem. B 108 (2004), pp. 13656–13666.

[46] O. Cairon, T. Chevreau, and J.-C. Lavalley, *Bronsted acidity of extraframework debris in steamed Y zeolites from the FTIR study of CO adsorption*, J. Chem. Soc. Far. Trans. 94 (1998), pp. 3039–3047.

[47] P. Gallezot, *Preparation of metal clusters in zeolites*, Mol. Sieves 3 (2002), pp. 257–305.

[48] K. Seff, *Cationic zinc clusters with mean formula Zn6.9 + 5.4 in the sodalite cavities of zeolite Y (FAU)*, Microporous Mesoporous Mater. 85 (2005), pp. 351–354.

[49] M. Calligaris, A. Mezzetti, G. Nardin, and L. Randaccio, *Cation sites and framework deformations in dehydrated chabazites. Crystal structure of a fully silver-exchanged chabazite*, Zeolites 4 (1984), pp. 323–328.

[50] I.J. Drake, Y. Zhang, D. Briggs, B. Lim, T. Chau, and A.T. Bell, *The local environment of Cu^+ in Cu-Y zeolite and its relationship to the synthesis of dimethyl carbonate*, J. Phys. Chem. B 110 (2006), pp. 11654–11664.

[51] S.R. Stoyanov, J.M. Villegas, A.J. Cruz, L.L. Lockyear, J.H. Reibenspies, and D. P. Rillema, *Computational and spectroscopic studies of Re(I) bipyridyl complexes containing 2,6-dimethylphenylisocyanide (CNx) ligand*, J. Chem. Theory Comput. 1 (2005), pp. 95–106; J.E. Monat, J.H. Rodriguez, and J.K. McCusker, *Ground- and excited-state electronic structures of the solar cell sensitizer bis(4,4′-dicarboxylato-2,2′-bipyridine)bis(isothiocyanato)ruthenium(II)*, J. Phys. Chem. A 106 (2002), pp. 7399–7406.

[52] R.G. Pearson, *Hard and soft acids and bases*, J. Am. Chem. Soc. 85 (1963), pp. 3533–3539.

[53] R.G. Parr and W. Yang, *Density functional approach to the frontier-electron theory of chemical reactivity*, J. Am. Chem. Soc. 106 (1984), pp. 4049–4050.

[54] P.W. Ayers and R.G. Parr, *Variational principles for describing chemical reactions: The Fukui function and chemical hardness revisited*, J. Am. Chem. Soc. 122 (2000), pp. 2010–2018.

[55] K. Fukui, T. Yonezawa, and C. Nagata, *Theory of substitution in conjugated molecules*, Bull. Chem. Soc. Jap. 27 (1954), pp. 423–427.
[56] K. Fukui, *Role of frontier orbitals in chemical reactions*, Science 218 (1982), pp. 747–754.
[57] F.L. Hirshfeld, *Bonded-atom fragments for describing molecular charge densities*, Theor. Chim. Acta B 44 (1977), pp. 129–138, B. Delley, *Calculated electron distribution for tetrafluoroterephthalonitrile (TFT)*, Chem. Phys. Lett. 110 (1986), pp. 329–338.
[58] R.S. Mulliken, *Electronic population analysis on LCAO-MO [linear combination of atomic orbital-molecular orbital] molecular wave functions. I*, J. Chem. Phys. 23 (1955), pp. 1833–1840; R.S. Mulliken, *Electronic population analysis on LCAO-MO [linear combination of atomic orbital-molecular orbital] molecular wave functions. II. Overlap populations, bond orders, and covalent bond energies*, J. Chem. Phys. 23 (1955), pp. 1841–1846.
[59] R.K. Roy, K. Hirao, S. Krishnamurthy, and S. Pal, *Mulliken population analysis based evaluation of condensed Fukui function indices using fractional molecular charge*, J. Chem. Phys. 115 (2001), pp. 2901–2907.
[60] V.V. Mihaleva, R. van Santen, and A.P.J. Jansen, *Quantum chemical calculation of infrared spectra of acidic groups in chabazite in the presence of water*, J. Chem. Phys. 119 (2004), pp. 13053–13060.
[61] S.P. Yuan, J.G. Wang, Y.W. Li, and S.Y. Peng, *Theoretical studies on the properties of acid site in isomorphously substituted ZSM-5*, J. Mol. Catal. A 178 (2002), p. 267.
[62] A.L. Sargent and E.P. Titus, *C—S and C—H bond activation of thiophene by Cp*Rh(PMe3): A DFT theoretical investigation*, Organometallics 17 (1998), p. 65.
[63] F. Li, L. Song, L. Duan, X. Li, and Z. Sun, *A frequency response study of thiophene adsorption in zeolite catalysts*, Appl. Surf. Sci. 253 (2007), pp. 8802–8809.
[64] P. Mills, S. Korlann, M.E. Bussell, M.A. Reynolds, M.V. Ovchinnikov, R.J. Angelici, C. Stinner, T. Weber, and R. Prins, *Vibrational study of organometallic complexes with thiophene ligands: Models for adsorbed thiophene on hydrodesulfurization catalysts*, J. Phys. Chem. A 105 (2001), pp. 4418–4429.